minerals

MDPI

Article

Accumulation of Platinum Group Elements in Hydrogenous Fe–Mn Crust and Nodules from the Southern Atlantic Ocean

Evgeniya D. Berezhnaya [1,*], Alexander V. Dubinin [1], Maria N. Rimskaya-Korsakova [1] and Timur H. Safin [1,2]

[1] Shirshov Institute of Oceanology, Russian Academy of Sciences, 36, Nahimovskiy prt., 117997 Moscow, Russia; dubinin@ocean.ru (A.V.D.); korsakova@ocean.ru (M.N.R.-K.); timursafin@list.ru (T.H.S.)

[2] Institute of Chemistry and Problems of Sustainable Development, D. Mendeleev University of Chemical Technology of Russia, 9, Miusskya Sq., 125047 Moscow, Russia

* Correspondence: evgeniya.berezhnaya@gmail.com; Tel.: +7-4991-245-949

Received: 27 May 2018; Accepted: 25 June 2018; Published: 28 June 2018

Abstract: Distribution of platinum group elements (Ru, Pd, Pt, and Ir) and gold in hydrogenous ferromanganese deposits from the southern part of the Atlantic Ocean has been studied. The presented samples were the surface and buried Fe–Mn hydrogenous nodules, biomorphous nodules containing predatory fish teeth in their nuclei, and crusts. Platinum content varied from 47 to 247 ng/g, Ru from 5 to 26 ng/g, Pd from 1.1 to 2.8 ng/g, Ir from 1.2 to 4.6 ng/g, and Au from less than 0.2 to 1.2 ng/g. In the studied Fe–Mn crusts and nodules, Pt, Ir, and Ru are significantly correlated with some redox-sensitive trace metals (Co, Ce, and Tl). Similar to cobalt and cerium behaviour, ruthenium, platinum, and iridium are scavenged from seawater by suspended ferromanganese oxyhydroxides. The most likely mechanism of Platinum Group Elements (PGE) accumulation can be sorption and oxidation on δ-MnO_2 surfaces. The obtained platinum fluxes to ferromanganese crusts and to nodules are close and vary from 35 to 65 ng·cm^{-2}·Ma^{-1}. Palladium and gold do not accumulate in hydrogenous ferromanganese deposits relative to the Earth's crust. No correlation of Pd and Au content with major and trace elements in nodules and crusts have been identified.

Keywords: Fe–Mn crust and nodules; platinum group elements; gold; Atlantic Ocean

1. Introduction

Ferromanganese crusts and nodules are considered to be the most important resource of metals in the ocean; mining of these deposits has been widely discussed, for example, in [1–3]. Platinum accumulates in nodules and crusts, and its content amounts up to 1–3 ppm [4,5]. Palladium concentrations in seawater are similar to platinum, but Pd does not accumulate in ferromanganese crusts and nodules [6,7]. There is much less data on the distribution and behaviour of ruthenium and iridium [8,9]. Relative to the platinum group element (PGE) concentrations in seawater and the Earth's crust, the ferromanganese crusts are enriched in these elements in the following order: Ir > Ru > Pt > Pd [10]. Platinum accumulates in the oxyhydroxide minerals of the nodules [11]. Depending on the mechanism of formation, Fe–Mn nodules can be classified as hydrogenous and diagenetic. Hydrogenous nodules grow slowly due to direct precipitation of colloidal particles of Fe–Mn oxyhydroxides from seawater. In diagenetic nodules, the source of manganese, iron, and the minor elements is an accretion of Fe–Mn oxyhydroxide colloids dissipated in sediments (oxic diagenesis) or pore water of underlying sediments due to the destruction of organic matter (suboxic diagenesis). Ferromanganese nodules form on the sediment–water interface and always contain diagenetically reworked material [12]. Unlike the nodules, the main source of hydrogenous

ferromanganese crusts is Fe–Mn oxyhydroxides precipitated from the water column. Fe–Mn oxyhydroxides supplied with hydrothermal fluid to the bottom water compose hydrothermal crusts. Hydrogenous deposits consist primarily of Fe-vernadite. Their typical Mn/Fe ratio is close to 1 and they are enriched with Co, rare earth elements, Y, and Te. In contrast, the main minerals in diagenetic nodules and hydrothermal crusts are asbolane-buzerite, birnessite, and todorokite. These deposits typically demonstrate increased contents of Ni, Cu, and Ba [13]. The Mn/Fe ratio in diagenetic nodules is usually higher than 2.5. It is well known that platinum accumulates in various types of ferromanganese deposits differently. Its concentrations decrease in the following order: hydrogenous crusts > hydrogenous nodules > diagenetic nodules > hydrothermal crusts [14,15].

Recent advances in analytical methods have led to an increasing number of studies related to PGE distribution in ferromanganese crusts [10,16–21]. Relatively few publications concern the PGE content in ferromanganese nodules [14,15,17]. Until recently, there has been no consensus about the sources of platinum group elements and mechanism of their accumulation. Seawater is assumed to be the main source of platinum for hydrogenous ferromanganese deposits. It is suggested that these elements are incorporated due to sorption and subsequent redox reactions on ferromanganese oxyhydroxides [6,10,14,22,23]. Also, it was assumed that the enrichment of Fe–Mn crusts with platinum results from the incorporation of fine-grained particles of noble metals [24–26]. Another reason for Pt accumulation in the hydrogenous crusts is its association with organic ligands in seawater [27].

In the case of PGE accumulation on ferromanganese oxyhydroxides from seawater via oxidative reaction, their distribution should be linked with other elements with the same source and supply mechanism (Mn, Co, Tl, and Ce). In contrast, incorporation of noble metal particles would result in the irregular distribution of PGE among ferromanganese samples and in the absence of a relationship between PGE and other trace and major elements. In this work, the behaviour of platinum group elements (Ru, Pd, Ir, and Pt) and gold in hydrogenous ferromanganese crusts and nodules from the Cape and Brazil Basins of the Atlantic has been considered. Samples were chosen to show PGE variations within the sample, station, basin, and oceanic region. Also, we included Fe–Mn crusts from the same stations to compare the accumulation of platinum group elements between different types of ferromanganese deposits. New PGE content data were presented together with mineralogical, chemical, and geochronological analysis to discuss the reason for platinum enrichment in Fe–Mn deposits.

2. Regional Setting

Brazil Basin is located between the continental slope of Brazil and the Mid-Atlantic Ridge (MAR) and extends from north to south for 3000 km at a water depth of more than 4000 m (Figure 1). Formation of the Basin was followed by strong volcanic activity. Relief of the Brazil Basin floor includes seamounts, ridges, depressions, and valleys. Stratified sediments have a thickness of 100–400 m and fill up depressions and valleys between ridges. The Cape Basin is situated between the Walvis and Agulhas Ridges and borders the MAR on the west. On the floor of the Cape Basin, there are numerous seamounts [28].

Both Basins are situated under the anticyclone gyre formed by the Benguela, South Equatorial, Brazil, and South Atlantic Currents. Three major subsurface water masses are governed by Circumpolar Water. Antarctic surface water masses descend to form Antarctic Intermediate Water (AAIW) that spreads to the north between 500 and 1000 m water depth. Above this, warm and salty South Atlantic Central Water is located. Upper Circumpolar Deep Water (UCDW) is the deepest water mass of the upper ocean, with a net northward transport [29]. The deep and abyssal water masses are the North Atlantic Deep Water (NADW) and the Antarctic Bottom Water (AABW). The NADW is transported into the South Atlantic predominantly in the deep western boundary current (DWBC) along the Brazilian continental slope. The NADW is located underneath the Upper Circumpolar Deep Water between about 1200 m and 3900 m in the tropics and between 1700 and 3500 m in the subtropics.

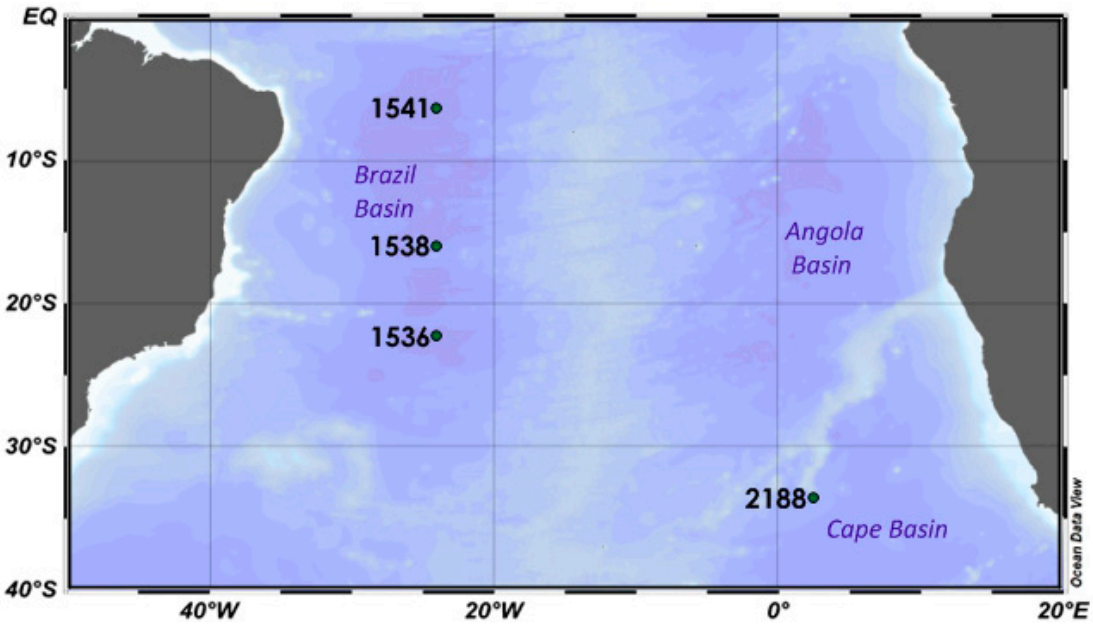

Figure 1. Location of crust and nodule samples.

The AABW enters from the south in the Cape Basin, and in the Brazil Basin, it penetrates through Rio Grande gaps. AABW is distributed in both Basins at depths greater than 3800 m [30]. AABW is cold and undersaturated with calcium carbonate. Carbonate compensation depth (CCD) is located at the depth of 4800–5000 m in the Brazil Basin and at the depth of 5100 m in the Cape Basin. Anticyclone circulation leads to water descending, which results in a low biological productivity of its surface water and low sedimentation rates [31]. Below the CCD, in both Basins, red pelagic clays are widely distributed. Sediments of the Brazil Basin have high iron and manganese contents, which could result from volcanic activity in the past [32].

3. Materials and Methods

Samples were collected during cruise 18 of the Research Vessel *Akademik Sergey Vavilov* (2004) and cruise 29 of the Research Vessel *Academik Ioffe* in 2009 (Figure 1, Table 1).

Table 1. Coordinates, water depth, and exploration tools used for sampling.

Station	Coordinates		Depth (m)	Sampling
	Latitude	Longitude		
1536	22°17.6′ S	24°01.1′ W	5500	Gravity corer
1538	15°52.9′ S	24°04.6′ W	5200	Gravity corer
1541	6°10.8′ S	24°01.1′ W	5800	Gravity corer
2188	33°41.3′ S	2°31.48′ E	4700	Sigsbee trawl

Cores of sediments were collected using a gravity corer in the Brazil Basin at stations 1536 and 1541. Ferromanganese nodules were found on the sediment–water interface and at the depth of 418 and 83 cm below the seafloor, respectively (Figure 2, Table 2). At station 1538, a crust on basalt substrate was recovered. Sampled at station 2188 in the Cape Basin were a spherical ferromanganese nodule, three Fe–Mn nodules with fish teeth in their nuclei, and a thin crust on the honeycombed substrate. The sizes of the nodules and the crust are shown in Table 2. The spherical nodule was subdivided into two samples: the outer black layer (0–3 mm) and the inner grey layer (3–15 mm). From the biomorphous nodules, the teeth forming the nuclei were withdrawn, and only the oxyhydroxide layers

were analysed in this work. The honeycombed substrate of crust Cr 2188 was pumice changed to clayey minerals yellow-whitish in colour.

Mineral composition was determined by X-ray diffraction using a Rigaku D/MAX 2200 diffractometer with CuKα radiation (Rigaku Corporation, Tokyo, Japan). Diffraction patterns were collected from $2\theta = 5^\circ$ to 60°. Determination of platinum group elements (Ru, Pd, Ir, and Pt) and gold has been carried out by the method of mass spectrometry with inductively coupled plasma (ICP-MS) using Agilent 7500a (Agilent Technologies, Santa Clara, CA, USA) after preliminary concentration on anionite Dowex 1×8 [33]. The standard addition method has been applied to eliminate losses during chromatography. The accuracy and precision of PGE concentration data have been checked using reference sample NOD-P-1. Analysis of magnesium and rare earth and trace elements has been carried out using the ICP-MS method after sample acid digestion [34]. Fe, Mn, Ti, and Al have been analysed applying the method of atomic absorption spectrometry (AAS) using SpectrAA 220 (Varian) (Varian Australia Pty Ltd, Victoria, Australia). The P content was determined by the spectrophotometric method with a precision of 3%. The precision of ICP-MS and AAS analyses varied within the limits of 3–5%. The accuracy of determination methods was controlled using reference samples: basalt (BCR-1, BCR-2), andesite (AGV-1), and Fe–Mn nodule (NOD-P-1, OOPE-601 and OOPE-602). The ages of the teeth from nodule 2188-Th4 and from surface sediments were determined using the method of strontium isotopic stratigraphy (SIS) [35] described in previous works [36,37]. The rate of ferromanganese crust growth was estimated by cobalt chronometer in accordance with the equation: $V\ (mm \cdot Ma^{-1}) = 0.68/[Co]^{1.67}$ [38,39].

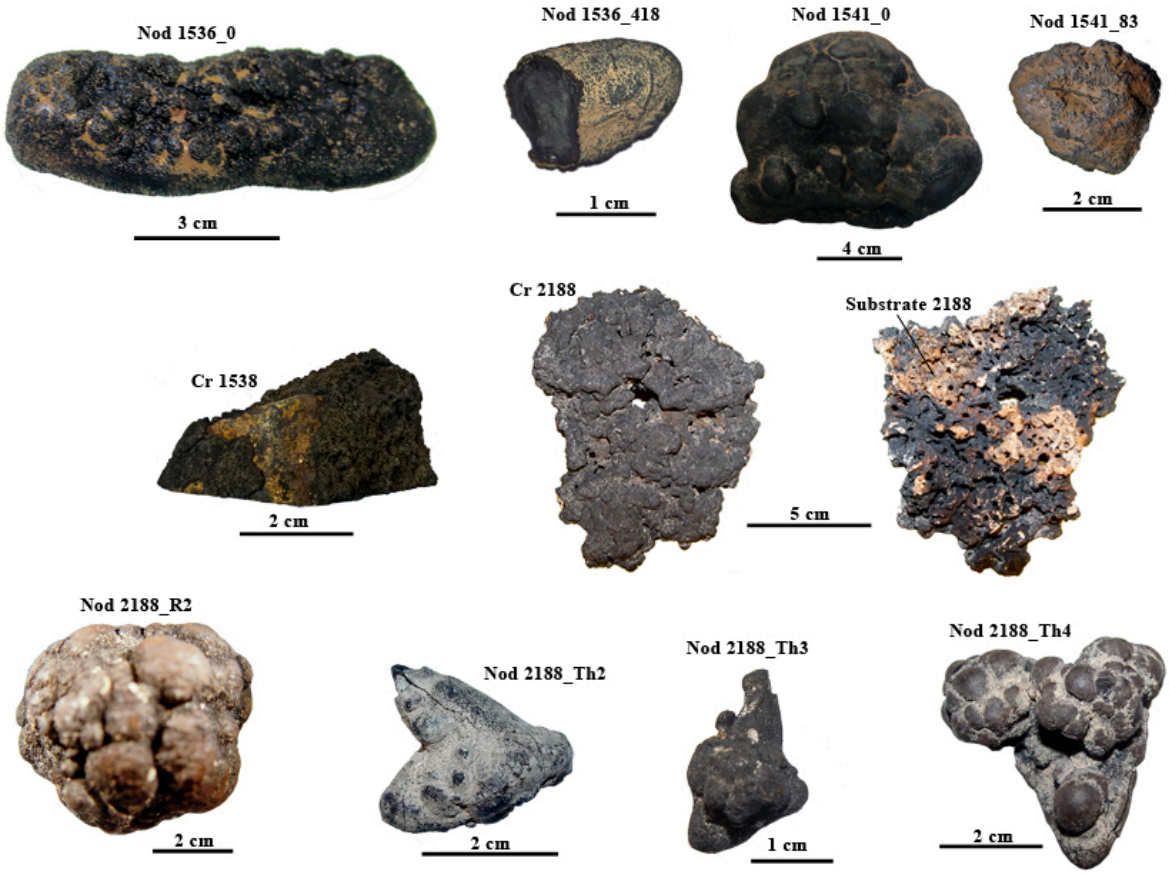

Figure 2. Photographs of the crust and nodules from the Brazil and Cape Basins.

Table 2. Sample description.

Sample	Description	Main Minerals (Minor Minerals)
Nod 1536_0	Black Fe–Mn nodule 85 × 35 × 20 mm in size with rugged surface and disc-like extended shape	Buserite-2 (asbolane-buserite)
Nod 1536_418	Buried nodule 23 × 15 × 11 mm in size	Buserite-2, Fe-vernadite (asbolane-buserite, birnessite, goethite)
Nod 1541_0	Polynuclear ferromanganese nodule with rugged black surface 115 × 85 × 60 mm in size	Buserite-2, Fe-vernadite (asbolane-buserite, birnessite)
Nod 1541_83	Buried nodule 45 × 30 × 7 mm	Feroxyhyte, goethite (Fe-vernadite, hematite)
Cr 1538	Fe–Mn crust 2–3 mm thick on basalt fragment	Fe-vernadite, feroxyhyte (quartz)
Nod 2188-R2_0-3	Spherical nodule 37–41 mm in diameter, outer black layer 0–3 mm from surface	Fe-vernadite, feroxyhyte (vernadite, asbolane-buserite, buserite-1, birnessite)
Nod 2188-R2_3-15	Spherical nodule 37–41 mm in diameter, grey layer 3–15 mm from surface	Fe-vernadite, feroxyhyte (vernadite, asbolane-buserite, nontronite)
Nod 2188-Th2	Biomorphous nodules 24 × 16 × 16 mm, oxyhydroxide layers 1.5–3 mm thick	Fe-vernadite, feroxyhyte (vernadite, asbolane-buserite, nontronite)
Nod 2188-Th3	Biomorphous nodules 20 × 12 × 12 mm, oxyhydroxide layers 1–3 mm thick	Fe-vernadite, feroxyhyte (vernadite, asbolane-buserite, nontronite)
Nod 2188-Th4	Large biomorphous nodule 43 × 41 × 29 mm with shark teeth in nuclei, oxyhydroxide layers 3–14 mm thick	Fe-vernadite, feroxyhyte (vernadite, asbolane-buserite, nontronite)
Cr 2188	Fe–Mn crusts 3−10 mm thick	Fe-vernadite (quartz, plagioclase)
Sub 2188	The substrate of Cr 2188, a fragment of porous pumice transformed into zeolite and clay	Phillipsite, clay (quartz, plagioclase)

4. Results

The mineral composition of the studied crusts and nodules consists predominantly of Fe-vernadite and X-ray amorphous iron oxyhydroxide (feroxyhyte). Some nodules contain a moderate amount of 10 Å manganate minerals (buserite, asbolane-buserite), which could reflect diagenetic Mn contribution. Mineral composition of the buried nodule 1541_83 was described by Dubinin et al. [36]. Manganese minerals were replaced along with the periphery of columnar framboids by low crystallized goethite FeOOH (Figure 3) with relict growth structures.

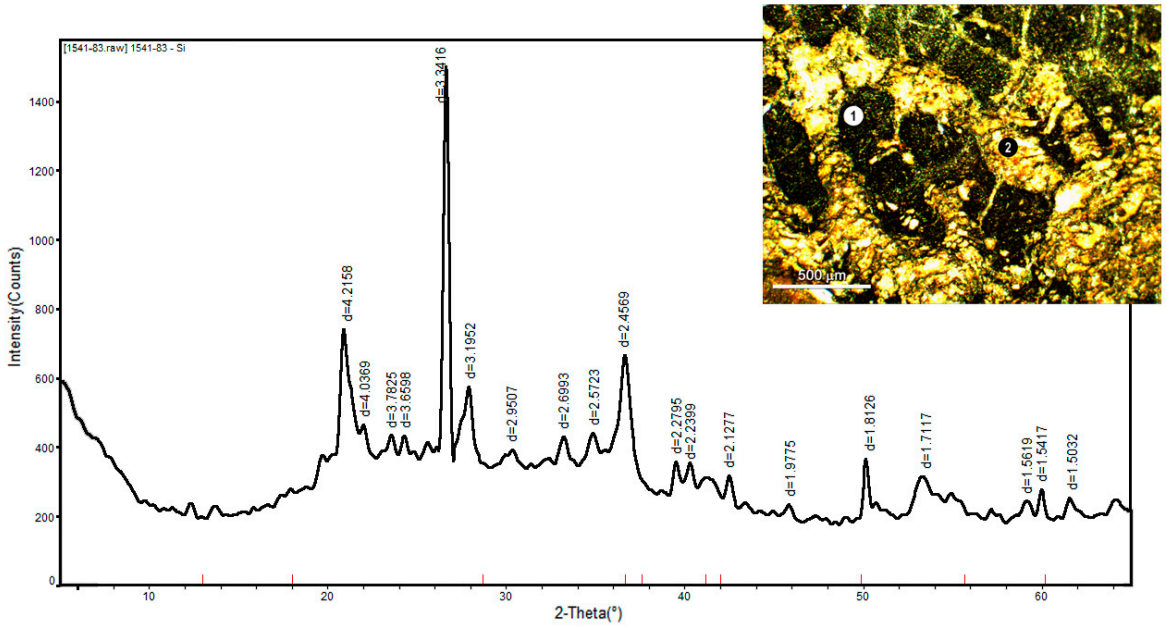

Figure 3. X-ray diffraction analysis pattern of the buried nodule 1541_83 and the reflected light image of its inner part. Inset: Fe-vernadite (**1**) is replaced by goethite (**2**).

The chemical composition of the studied ferromanganese samples is presented in Table 3. Surface ferromanganese nodules from the Brazil Basin and the buried nodule from station 1536 are close in their compositions. Mn contents vary from 17.8% to 19.7%; Fe from 13.7% to 15.1%; Co from 0.16% to 0.21%; Ni from 0.54% to 0.77%; Cu from 0.26% to 0.29%. The buried nodule nod 1541_83 is unique in its composition with Mn/Fe ratio of 0.41 together with Fe enrichment (23.5%). This nodule is depleted in copper, nickel, cobalt, and zinc relatively to the nodule on the surface sediments [36]. The Ce anomaly value reaches 41 (normalized to Post Archean Australian Shale (PAAS)), because the contents of trivalent rare earth elements are too low (Figure 4). The crust from station 1538 has a Mn/Fe ratio = 1.2; it is also enriched with cobalt and cerium. Mn/Fe ratios in the nodules of the Cape Basin vary from 1.0 to 1.6. Cobalt, nickel, and copper contents are lower than in Brazil Basin nodules. The crust from station 2188 is similar to nodules in its composition. As compared with nodules, it contains less lithium, copper, and nickel. The cerium anomaly (Ce an) is 3.4. On the ternary diagram in coordinates of Fe–Mn-10(Co + Ni + Cu) [40], the studied ferromanganese deposits from the Cape and Brazil Basins are located in the area of deep-sea pelagic nodules and crusts (Figure 5). The buried nodule from station 1541 and crust 2188 are the exceptions. Due to the low contents of Co + Ni + Cu, the buried nodule falls into a hydrothermal deposit area. Figure 6 shows the composition of rare-earth elements (REE) and yttrium in coordinates of Ce an−Nd and Ce an−$(Y/Y^{PAAS})/(Ho/Ho^{PAAS})$ [41]. The studied ferromanganese crusts and nodules are located in hydrogenous ferromanganese deposits area on the diagram, while the buried nodule from station 1541 is located off from the highlighted areas due to high Ce an value.

Table 3. Concentrations of major and trace elements of crust and nodules from the Cape and Brazil Basins.

Sample	Brazil Basin					Cape Basin						
	Nod 1536_0	Nod 1536_418	Nod 1541_0	Nod 1541_83	Cr 1538	Nod 2188-Th2	Nod 2188-Th3	Nod 2188-Th4	Nod 2188-R2 0-3	Nod 2188-R2 3-15	Cr 2188	Substrate 2188
Mn	17.8	19.7	18.6	9.3	18.0	17.7	16.9	13.9	16.9	14.2	13.5	0.8
Fe	15.7	13.1	15.7	23.5	15.1	12.4	10.4	13.7	14.4	13.0	16.3	2.9
Mn/Fe	1.1	1.5	1.2	0.4	1.2	1.4	1.6	1.0	1.2	1.1	0.8	0.3
Al	3.66	3.58	2.95	2.90	2.18	3.50	3.45	3.63	2.4	2.5	2.20	8.29
Mg	4.87	4.49	5.14	4.30	1.28	-	-	-	1.2	1.0	1.27	1.75
P	0.267	0.272	0.272	0.287	0.300	0.255	0.234	0.286	0.260	0.212	0.321	0.156
Ti	0.62	0.52	0.45	0.50	0.63	0.78	0.68	0.84	0.65	0.60	0.69	0.28
Li	126.3	144.0	101.2	8.5	43.4	81.9	89.2	36.4	43.9	30.0	16.5	95.4
Be	2.42	2.28	3.26	7.87	3.36	5.23	4.48	3.90	3.4	3.9	3.35	1.36
V	521	481	511	1177	605	416	368	441	459	418	561	53
Co	2048	2181	1617	1096	3263	1254	1176	1324	1556	1573	1538	56
Ni	6940	7665	5403	347	3616	4835	4917	3127	4197	2969	2022	528
Cu	2583	2879	2896	317	1353	2216	2396	1215	1641	1425	615	571
Zn	655	713	643	460	538	655	678	465	636	489	429	186
As	139	120	130	277	188	-	-	-	134	114	200	4
Rb	29.0	23.4	16.8	23.4	14.3	23.0	24.5	30.1	14.7	12.9	17.7	70.1
Sr	515	591	693	733	947	854	786	850	869	805	988	117
Y	87	76	93	13	86	122	103	116	128	127	127	89
Mo	377	422	416	508	385	-	-	-	212	239	187	11
Cd	8.4	9.8	8.3	0.9	4.1	6.4	6.5	4.0	5.8	4.5	2.9	0.4
Cs	1.8	1.1	1.1	0.6	0.8	1.0	1.0	1.0	0.8	0.7	0.9	3.0
Ba	1048	1183	1228	2072	985	835	845	879	869	947	739	190
W	72.0	75.5	48.1	19.8	42.3	-	-	-	32.2	40.3	24.6	1.6
Tl	121.0	130.2	89.0	20.3	157.9	148.0	145.8	90.7	150	132	52.4	4.9
Pb	565	688	690	1056	825	978	896	942	1191	1162	1290	25
Bi	7.8	8.4	7.0	6.6	-	-	-	-	17.6	20.6	-	-
Th	62.4	60.2	86.8	70.3	75.9	73.5	65.2	96.5	95.0	79.9	102.5	13.9
U	4.3	4.5	4.9	7.6	7.0	7.6	6.8	7.3	7.7	6.6	7.6	0.9
La	121	129	171	27	149	156	136	169	192	212	189	62
Ce	919	1072	1216	2108	2103	830	732	1079	1378	1667	1482	65
Pr	33.1	34.0	49.1	5.2	34.2	46.6	40.3	48.6	56.6	65.8	52.0	21.1
Nd	132.1	134.7	192.3	18.9	126.0	187.8	163.1	194.9	217	247	203.1	87.1
Sm	30.6	30.5	45.3	4.5	28.5	44.8	38.8	47.5	51.8	58.6	47.0	20.1

Table 3. *Cont.*

Sample	Brazil Basin					Cape Basin						
	Nod 1536_0	Nod 1536_418	Nod 1541_0	Nod 1541_83	Cr 1538	Nod 2188-Th2	Nod 2188-Th3	Nod 2188-Th4	Nod 2188-R2 0-3	Nod 2188-R2 3-15	Cr 2188	Substrate 2188
Eu	6.97	6.81	10.2	1.13	6.4	10.5	9.09	11.1	11.8	13.2	10.6	4.63
Gd	29.0	28.3	41.5	4.3	25.1	42.1	36.6	44.8	49.4	53.9	44.7	19.7
Tb	4.48	4.32	6.29	0.90	4.53	6.71	5.89	6.92	7.4	8.1	7.24	2.93
Dy	25.3	24.4	34.0	4.2	26.1	38.8	33.6	38.9	42.8	45.9	40.5	16.5
Ho	4.71	4.47	6.04	0.77	4.79	7.22	6.25	7.08	8.0	8.3	7.62	3.14
Er	12.7	11.9	15.8	2.3	13.8	20.2	17.2	19.5	20.9	21.8	19.4	8.3
Tm	1.82	1.74	2.27	0.37	2.01	2.91	2.49	2.78	2.8	2.9	2.56	1.05
Yb	11.5	11.0	14.1	2.5	14.5	18.5	16.1	17.6	18.2	19.3	17.5	6.7
Lu	1.82	1.71	2.23	0.42	2.28	2.77	2.35	2.60	2.8	2.9	2.69	1.01
Ce an	3.3	3.7	3.1	41.1	6.8	2.2	2.2	2.7	3.0	3.2	3.4	0.4
∑REY	1422	1570	1899	2193	2627	1537	1343	1806	2187	2554	2253	409
L/H	0.85	0.92	1.00	0.68	0.76	0.74	0.75	0.82	0.90	0.97	0.89	0.88

Contents of Mn–Ti are given in %, and the remaining elements in ppm. ∑REY = ∑REE+ Y. The Ce anomaly is calculated as Ce an = $2Ce/Ce^{PAAS}/(La/La^{PAAS} + Pr/Pr^{PAAS})$, $L/H = (La/La^{PAAS} + 2 \times Pr/Pr^{PAAS} + Nd/Nd^{PAAS})/(Er/Er^{PAAS} + Tm/Tm^{PAAS} + Yb/Yb^{PAAS} + Lu/Lu^{PAAS})$, where Ln^{PAAS} is the content in PAAS [42].

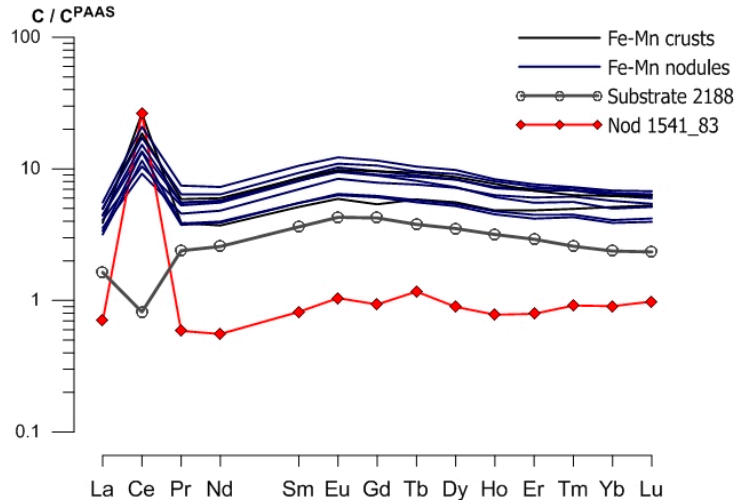

Figure 4. Normalized to Post Archean Australian Shale (PAAS) [42], the REE composition of studied ferromanganese nodules and crusts.

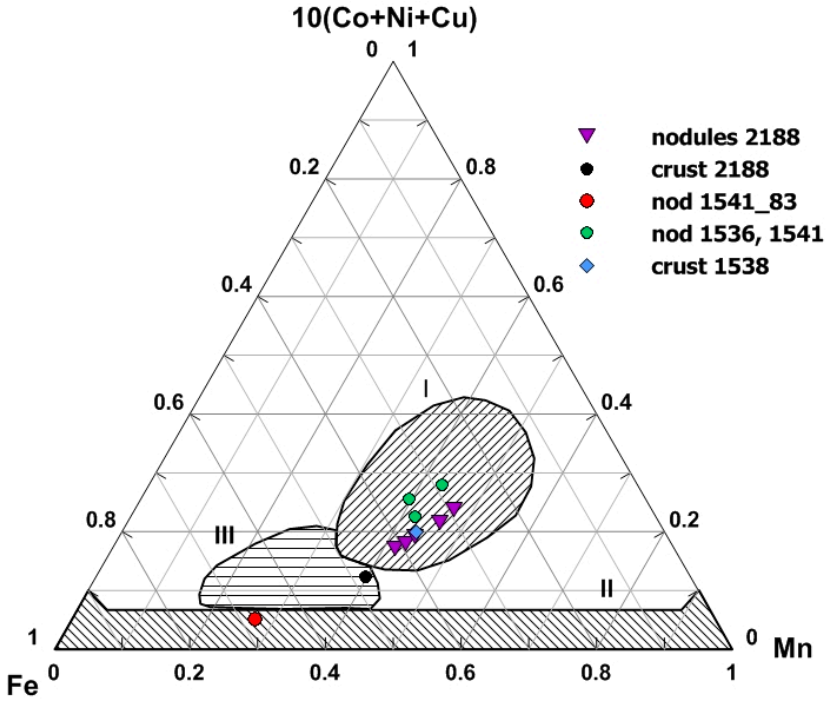

Figure 5. Ternary diagram of Bonatti et al. [40] showing nodule composition in Fe–Mn-10 × (Co + Ni + Cu) coordinates: (**I**) Field of deep-sea pelagic nodules and hydrogenous crusts; (**II**) field of hydrothermal Fe–Mn deposits; (**III**) field of hydrothermal metalliferous sediments and diagenetic nodules, from the margins of the oceanic pelagic zone.

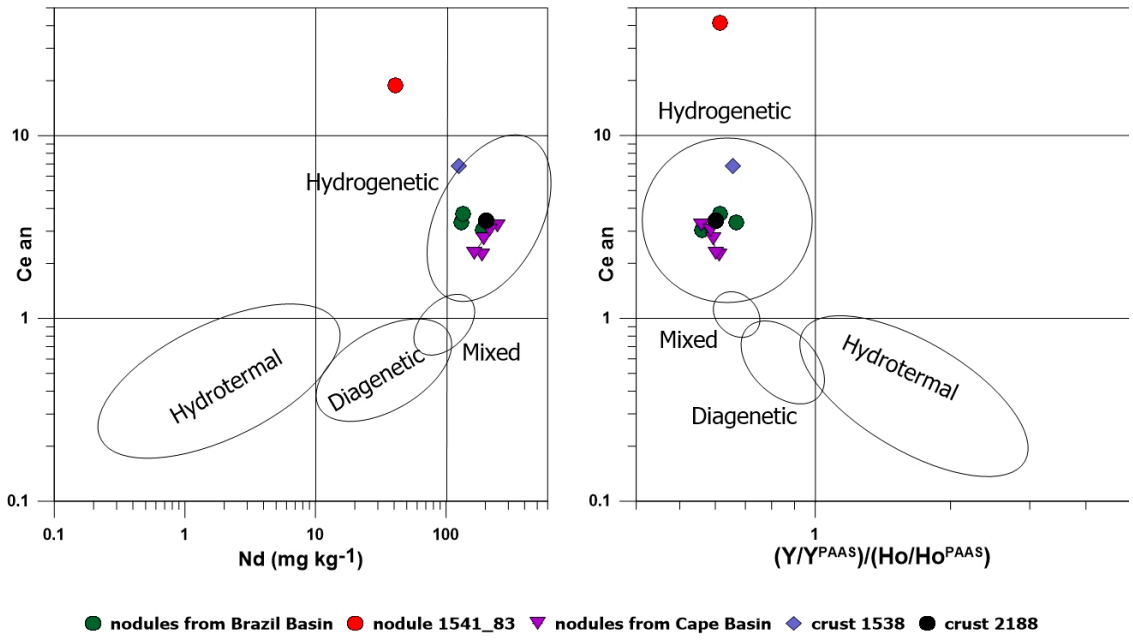

Figure 6. Composition of REE and Y in coordinates of Ce an−Nd and Ce an−$(Y/Y^{PAAS})/(Ho/Ho^{PAAS})$ [41] in studied crusts and nodules.

As a rule, platinum contents in hydrogenous ferromanganese deposits are higher by one to two orders of magnitude than those of other platinum group elements (Table 4). In the crust and nodules from the Brazil Basin, Pt concentrations vary from 110 ng/g to 247 ng/g. Comparison between the surface and buried nodules from station 1536 shows that the platinum and iridium contents

are practically the same. The buried nodule from station 1541 is enriched with platinum by more than twofold compared to the surface nodule. Its Pt content is higher than that in the crust from station 1538. In Brazil Basin ferromanganese deposits, Ru contents vary from 9.5 to 19 ng/g and Ir from 1.2 to 4.6 ng/g. For the samples from the Cape Basin, the highest contents of PGEs have been found in the spherical nodule from station 2188. In the outer (black) and inner (grey) layers, the contents of platinum, ruthenium, iridium, and palladium are practically the same. The nodules with the teeth in the nuclei contained 78–80 ng/g of platinum. The lowest platinum content was found in the crust from station 2188 (47 ng/g). Palladium contents vary in the studied crusts and nodules from 1.1 to 2.8 ng/g, reaching maximum values in the crust substrate of 3.1 ng/g. Gold varies from <0.2 to 1.2 ng/g; no relation of it with major and trace elements has been revealed.

Table 4. PGE content (ng/g) in ferromanganese crust and nodules from the Cape and Brazil Basins.

	Sample	Ru	Pd	Ir	Pt	Au
Brazil	Nod 1536_0	9.5	2.1	3.3	161	0.3
Basin	Nod 1536_418	19.3	1.1	3.3	174	<0.2
	Nod 1541_0	13.7	1.3	1.2	110	<0.2
	Nod 1541_83	16.2	2.8	3.4	247	0.2
	Cr 1538	16.7	1.8	4.6	184	0.3
Cape	Nod 2188-Th2	-	-	1.7	79	<0.2
Basin	Nod 2188-Th3	-	-	1.4	78	<0.2
	Nod 2188-Th4	9.9	1.6	2.1	80	1.2
	Nod 2188-R2_0-3	25.9	1.4	2.2	107	<0.2
	Nod 2188-R2_3-15	22.3	2.0	3.2	105	<0.2
	Cr 2188	5.3	1.3	1.4	47	0.8
	Sub 2188	0.2	3.1	<0.2	6	0.8
	Seawater [43]	2×10^{-6}	60×10^{-6}	0.1×10^{-6}	50×10^{-6}	9.8×10^{-6} *
	Pelagic sediments [44]	-	8.0	-	9.5	1.4
	Earth crust [45]	0.1	0.4	0.05	0.4	2.5
	MORB [46]	0.103	1.5	0.04	0.6	0.7 **
	CI chondrite [47]	710	550	455	1010	140

* [48], ** [49], MORB: Mid-ocean ridge basalt.

The age of the surface sediments of station 1541 is evaluated as 24.1 Ma [36]. Assuming the age of nodule 1541_0 does not exceed the age of underlying sediments, its growth rate equals 1.2–2.4 mm·Ma^{-1}. The age of the tooth inside nodule 2188-4 (SIS) is estimated as 5.2 ± 0.2 Ma [35]. We have calculated the minimum possible growth rate of ferromanganese nodules (Table 5). Based on the growth rate, Pt fluxes (F) in ferromanganese deposits were calculated using the formula F = CGD, where C is concentration, D is density in situ (accepted as 1.6 g/cm^3), and G is the growth rate [50].

Table 5. Growth rates and Pt fluxes in investigated crust and nodules.

Sample	Growth Rate (mm·Ma^{-1})	Pt Flux (ng·cm^{-2}·Ma^{-1})
Nod 1541_0	2.4	42.2
Nod 2188-Th4	2.8	35.2
Cr 1538	2.2	64.8
Cr 2188	6.5	48.9

5. Discussion

5.1. Variations of PGE Contents in Nodules and Crusts

In hydrogenous nodules of the Pacific Ocean, platinum content varies from 83 ng/g [15] to 674 ng/g [14]. The PGE concentrations in the nodules of the Atlantic Ocean are within the same range, but they are lower than average values for the Pacific. Platinum concentrations in the two crusts are lower than average concentrations in the crusts from the Pacific, Indian, and Atlantic

oceans [10,15–21,51]. It should be noted that the number of studied samples from the Atlantic Ocean is not sufficient to make conclusions on the contents of platinum elements in ferromanganese ores of the Atlantic. Nevertheless, the observed PGE concentrations are consistent with the general trend of the lower redox-sensitive element concentration in Fe–Mn oxyhydroxides of the Atlantic compared to the Pacific Ocean [52]. In general, PGE contents in crusts are higher than in nodules. Gold and palladium do not accumulate in the oxyhydroxide part of ferromanganese crusts and nodules because their contents in crust substrate are equal or even higher than in crusts.

There is no significant difference in the contents of platinum group elements in the nodules between the Cape and Brazil Basins. Nevertheless, PGEs have smaller variations in the samples from one Basin than in samples from different Basins. Correlation analysis carried out for all studied nodules (except buried nodule Nod 1541_83) shows the significant correlation coefficients for the following pairs of elements: Pt–Co (R = 0.99), Ir–Co (R = 0.74), Ru–Tl (R = 0.79), and Ru–Ce (R = 0.74) (Table A1). Figure 7a shows platinum content dependence on cobalt in the studied ferromanganese crusts and nodules.

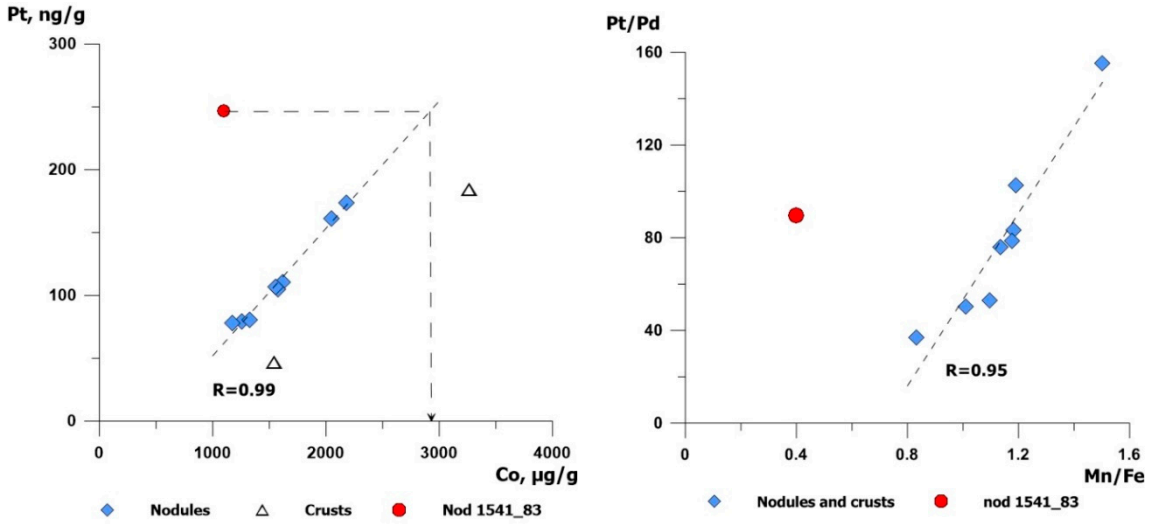

Figure 7. The relationship between Pt and Co (**a**) and Pt/Pd and Mn/Fe (**b**) in crusts and nodules from the Cape and Brazil Basins.

For all nodule samples, with the exception of the buried nodule from station 1541, a strong correlation between Pt and Co (R = 0.99) is observed. As has been already noted, platinum correlates with redox-sensitive elements (Co and Ce) which is highly enriched in hydrogenous ferromanganese deposits [10,14]. Co and Ce are incorporated in Fe–Mn oxyhydroxides during oxidation in surface seawater. Mn oxides oxidize Co(II) and Ce(III) to poorly soluble Co(III) and Ce(IV); also, FeOOH can oxidize Ce(III). In the ocean, platinum exists in two oxidation states, Pt(II) and Pt(IV), in the form of two complexes: $PtCl_4^{2-}$ and $PtCl_5OH^{2-}$ [53]. Although sorption of negatively charged particles on the negatively charged surfaces of δ-MnO_2 contradicts the electrochemical model [54], experimental studies confirm sorption and subsequent oxidation of platinum (Pt(II) → Pt(IV)) on manganese oxide [23,55]. We have observed a significant correlation (R = 0.95) between Pt/Pd and Mn/Fe ratios (Figure 7b) in our nodule and crust samples. The Pt/Pd ratio can be considered as the extent of platinum accumulation respectively to that of palladium and reflects the process of these elements' fractionation during hydrogenous accumulation. Thus, in seawater, Pt/Pd equals approximately 1, and grows in the following order: hydrothermal crusts < diagenetic nodules < hydrogenous nodules < hydrogenous crusts, from 7 to 407 [14]. Generally, the Mn/Fe ratio is a geochemical indicator of the source of matter in ferromanganese deposits. This ratio is sensitive for the Mn supply of hydrothermal

or diagenetic origin. Yet, within the narrow range of values typical for hydrogenous ferromanganese deposits (Mn/Fe = 0.8–1.5), this value also determines the ratio of Mn and Fe oxyhydroxides in the hydrogenous material. Platinum accumulation grows with an increase of the manganese oxide component in the hydrogenous ferromanganese deposits, which can implicitly indicate a possible association of Pt exactly with Mn. Experiments fulfilled by Kubrakova [27] showed that platinum (II) sorbs more effectively on a mixture of ferromanganese oxyhydroxides than on iron oxyhydroxides and manganese oxides separately. Apparently, the positively charged iron oxyhydroxides are involved in the Pt sorption process.

Cobalt and cerium behaviour in ferromanganese deposits is studied well, and the incorporation mechanism has been confirmed by experiments [56,57]. To compare platinum accumulation relatively to Co and Ce in different types of ferromanganese nodules, we have plotted their compositions onto the ternary diagram in Co–Ce–Pt $\times$ 10^4 coordinates (Figure 8). As well as our data, it shows published data on the contents of cobalt, platinum, and cerium in other nodule samples [14,15,17], including reference samples (see the legend). Based on the values of the Mn/Fe ratio in the nodules, we have distinguished the diagenetic and hydrogenous nodules (hydrogenous nodules: Mn/Fe < 2.5; diagenetic: Mn/Fe > 2.5). Separately, the nodules of marginal seas have been also plotted. They included the nodules from the South China Sea [17], reference sample NOD-A-1, and two nodules obtained in the Tasmanian Sea and described by [15]. According to the Mn/Fe ratio, these nodules are hydrogenous. Ferromanganese nodules of the Brazil and Cape Basins are located in the same field on the diagram, which we have determined as the nodule area of the Atlantic Ocean. The diagram shows the hydrogenous nodules of the Atlantic and Pacific Oceans in the different areas, since ferromanganese deposits of the Pacific Ocean contain more cobalt [52].

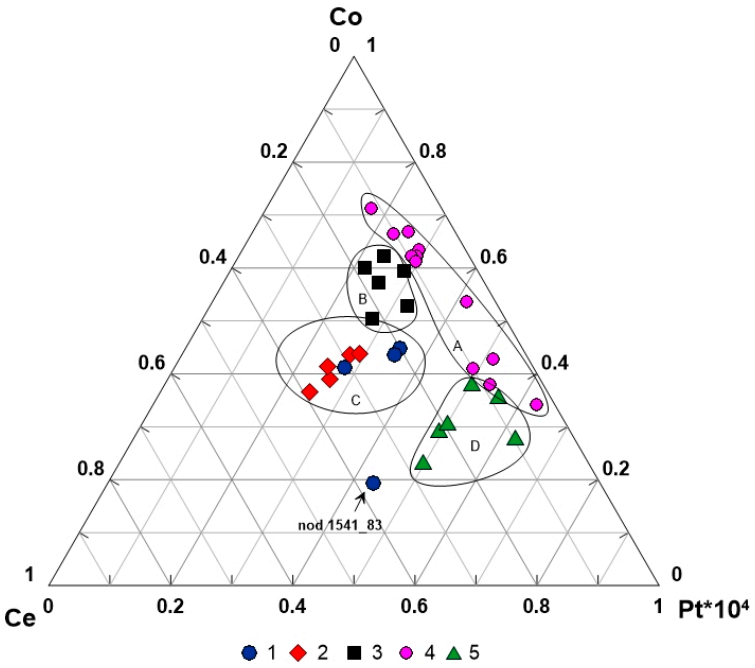

Figure 8. Ternary diagram showing nodule composition in Co–Ce–Pt $\times$ 10^4 coordinates: A—field of diagenetic nodules from the Pacific Ocean, B—field of hydrogenous nodules from the Pacific Ocean, C—field of hydrogeneous nodules from the Atlantic Ocean, D—field of marginal sea nodules. 1—nodules from the Brazil Basin (except nod 1541_83); 2—hydrogenous nodules from the Cape Basin; 3—hydrogenous nodules from the Pacific Ocean [14,15], reference samples GSPN-2, OOPE-601, OOPE-603; 4—diagenetic nodules [14,15], reference samples JMn-1, NOD-P-1, GSPN-3, OOPE-602; 5—marginal sea nodules [15,17].

All the diagenetic nodules shown are from the Pacific Ocean. They form an elongated area, which is related to the variable contents of platinum respective to the constantly high value of the Co/Ce ratio. Ferromanganese nodules of marginal seas show high platinum contents at relatively low cobalt and cerium concentrations. In the nodule samples, iridium-like platinum is significantly linked with cobalt, while ruthenium correlates better with cerium and thallium, which is oxidized on Fe–Mn oxyhydroxides from Tl(I) to Tl(III) (Table A1). As consistent with the stability constants, iridium and ruthenium can be in two states of oxidation: +3 and +4 [8]. The possible mechanism of enrichment for these elements might be oxidative sorption on suspended iron and manganese oxyhydroxides: Ir(III) → Ir(IV) and Ru(III) → Ru(IV).

5.2. Platinum Group Elements in Buried Nodules

Contents of PGEs in the two buried nodules from the Brazil Basin differ almost twofold. The buried nodule from the depth of 418 cm below the seafloor at station 1536 has a chemical composition close to that of the nodule from surface sediments. The plots of Pt versus Co show that the buried nodule 1536_418 composition lies along the trend line with the surface nodules (Figure 7a). Platinum content in nodule 1541_83 is significantly higher than in the buried nodule 1536_418 and in the surface nodules (Table 4). By its chemical composition, this buried nodule does not belong to any of genetic types of ferromanganese nodules. Diagenetic redistribution of matter that occurred after the nodule burial affected its composition significantly [36]. This led to partial Mn reduction and replacement of manganese minerals with goethite.

If one assumes that the ratios of cobalt and Mn/Fe to platinum in the buried nodule 1536_418 were the same as in other nodules, then the cobalt content in it had reached 0.3% and the Mn/Fe ratio was equal to 1.2 (Figure 7a,b). Such a chemical composition of the nodule is similar to other nodules of the Brazil Basin. Obviously, platinum accumulated in the nodules during their growth on the sediment surface. After the burial, manganese and trace elements related to manganese were lost, while platinum content remained unchanged. This passive platinum accumulation can indicate that it is not mobile under the early diagenesis conditions. Terashima et al. [44] did not reveal significant migration of Pt during early diagenesis, except in rare cases. Colodner et al. [58] showed redistribution of platinum and iridium during iron and manganese oxyhydroxide reduction in pelagic sediments. Apparently, platinum reduction occurs in sediments only at complete Mn and Fe oxyhydroxide reduction. The remaining manganese (IV) phases did not allow migration of platinum. In the case of nodule 1541_83, platinum turned out to be less mobile than cobalt during the partial dissolution of manganese oxyhydroxides and their replacement with goethite. Relatively low Pt concentrations observed in diagenetic nodules indicate both limited platinum migration during oxic diagenesis and the relatively high growth rate of diagenetic nodules [14].

5.3. Platinum Fluxes in Fe–Mn Crusts and Nodules

Possible sources of platinum group elements in the ocean can be riverine fluxes, hydrothermal processes, cosmic dust flux, and halmyrolysis of oceanic basalts. If riverine and cosmic inputs have been estimated in some works [59,60], the influence of hydrothermal process and basalt halmyrolysis are significantly less studied [61]. Ferromanganese deposits in the ocean are a significant sink of metals entering the ocean and indicate the source of the metal supply. Figure 9 shows PGEs in ferromanganese crusts and nodules normalised to CI chondrite. For comparison, the composition of platinum group elements in seawater and basalts of the Atlantic Ocean is also shown.

It is assumed that PGEs are supplied to ferromanganese crusts and nodules from seawater. Platinum elements in the ocean are not a chemically coherent group, and the seawater PGE composition is not inherited by ferromanganese deposits. Thus, palladium is mobile in seawater and its residence time in the ocean is longer (10–100 thousand years, [62]) than that of platinum (10–22 thousand years, [60]) and iridium (2–20 thousand years, [9]). Pd does not accumulate in ferromanganese deposits. On the contrary, iridium significantly enriches ferromanganese deposits relative to seawater

due to its preferential sorption on ferromanganese oxyhydroxides. Hence, Ru, Ir, and Pt enrich nodules by accumulating in their hydrogenous components. PGE distribution in hydrothermal crusts is similar to MORB composition, and Pd is less depleted relative to Pt in these deposits [14].

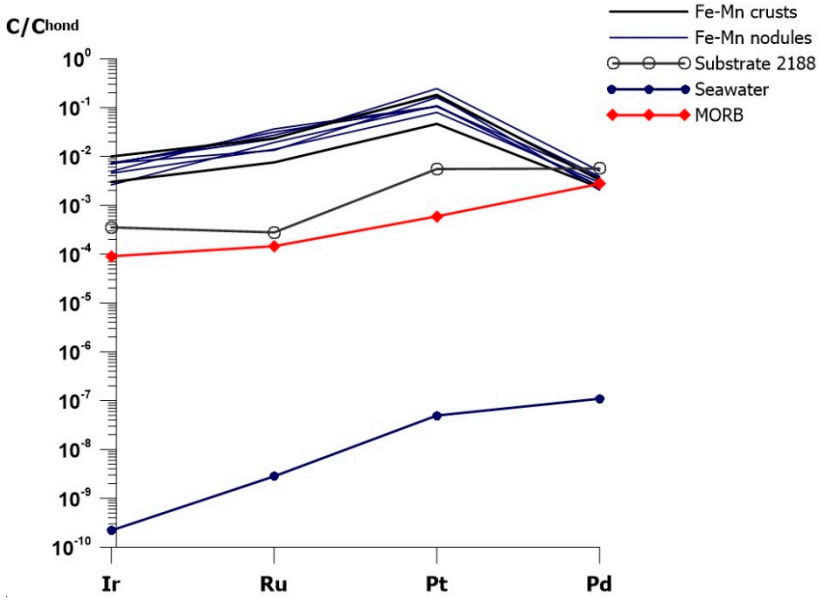

Figure 9. CI chondrite-normalized [47] PGE patterns in studied nodules, crust, and substrate. For comparison, the MORB [46] and seawater [43] PGE patterns are shown.

Platinum fluxes to ferromanganese crusts and nodules were found to be of the same order of magnitude (Table 5), although the methods of age determination were different. Calculated platinum flux into the nodules is lower than into the crusts. This effect is possibly related with a supply of diagenetic matter into the nodules, because the diagenetic matter is depleted of PGEs. The growth rate of crust Cr 2188 was found to be three times higher than that of Cr 1538, which explains the difference in Pt contents between the two crusts (47 versus 184 ng/g). Calculated platinum fluxes to these crusts differ less than by 15%. It confirms that platinum accumulation similar to that of cobalt and cerium depends primarily on the growth rate of ferromanganese crusts and nodules [38,63]. The lower the growth rate, the higher the platinum accumulation. Regardless of some differences in PGE contents in these deposits, accumulation of platinum in both crusts and nodules occurred due to the same process of sorption from seawater. Although it does not rule out other sources of PGE to ferromanganese crusts and nodules in the ocean, nevertheless, their influence has not been detected in the samples studied.

6. Conclusions

This study has investigated the behaviour of platinum group elements (Ru, Pd, Ir, and Pt) and gold in surface and buried deep-sea ferromanganese nodules of the Cape and Brazil Basins, together with the PGE composition of Fe–Mn crusts from both basins. Nodules and crusts show Mn/Fe ratio values ranging from 0.4 to 1.6, they are enriched with Co, display high positive anomaly values of Ce, and are hydrogenous in their origin. Platinum contents in the nodules from the Brazil Basin vary from 110 to 174 ng/g and generally are higher than those in the nodules from the Cape Basin (from 78 to 107 ng/g). There is no significant difference in concentrations of other PGEs and gold between both basins. Ru varies from 9 to 26 ng/g, Pd from 1.1 to 2.1 ng/g, Ir from 1.2 to 3.3 ng/g, and Au from less than 0.2 to 1.2 ng/g.

In the ocean, ruthenium, iridium, and platinum can change their oxidation state: Ru(+3) → Ru(+4), Ir(+3) → Ir(+4), and Pt(+2) → Pt(+4). Within ferromanganese nodules, they correlate with other redox-sensitive elements: Co, Ce, and Tl. This correlation indicates a similar mechanism of their

accumulation in ferromanganese deposits, namely surface oxidation of these elements when sorbed onto Fe–Mn oxyhydroxides. For palladium and gold, no relationship with major and trace elements have been revealed.

Platinum contents increase with the growth of the Mn/Fe ratio value in the studied hydrogenous crusts and nodules. It is probably related with platinum oxidation on the MnO_2 surface. The highest platinum content has been found in a buried nodule at the depth of 83 cm at station 1541 (Brazil Basin). During early diagenesis, the buried Fe–Mn nodule changed its composition, having lost a part of the manganese and manganese-related elements (Co, Ni, and Tl), while the platinum and cerium contents were retained. So, at preservation of Mn oxides within a nodule, Pt mobility in diagenesis is very limited. Based on strontium isotope stratigraphy and Co-chronometer methods, platinum fluxes in crusts and nodules have been estimated. Platinum fluxes are from 35–42 $ng \cdot cm^{-2} \cdot Ma^{-1}$ in nodules and 49–65 $ng \cdot cm^{-2} \cdot Ma^{-1}$ in crusts. Platinum fluxes in hydrogenous nodules were found to be somewhat lower than in crusts, because some admixture of the diagenetic material poor in PGE in Fe–Mn nodules is always contained. Given that the values of platinum fluxes in crusts and nodules are close, we can suggest that PGE accumulation occurs as a result of scavenging these elements from seawater.

Author Contributions: A.V.D. and E.D.B. had the original idea of this study. E.D.B. carried out PGE analysis, analyzed the data, and prepared the manuscript text. M.N.R.-K. and T.H.S. carried out chemical analysis of samples. A.V.D. revised the work.

Funding: This research was performed in the framework of IO RAS state assignment (theme No. 0149-2018-0015), supported by RFS (project No. 14-50-00095).

Acknowledgments: The authors wish to thank Anton Kuznetsov for providing geochronological data, and Tatyana Uspenskaya and Lubov Semilova for their help at different stages of the work.

Conflicts of Interest: The authors declare no conflict of interest. The founding sponsors had no role in the design of the study; in the collection, analyses, or interpretation of data; in the writing of the manuscript; and in the decision to publish the results.

Appendix A

Table A1. Correlation coefficient matrix for nodule samples from the Brazil and Cape Basins (except Nod 1541_83).

	Mn	Fe	Mn/Fe	Al	Li	Mg	Be	Ti	V	Co	Ni	Cu	Zn	As	Rb	Sr	Y	Mo	Cd	Cs	Ba	W	Tl
Mn	1.00																						
Fe	0.18	1.00																					
Mn/Fe	0.57	−0.70	1.00																				
Al	0.25	−0.16	0.33	1.00																			
Li	0.88	0.15	0.52	0.57	1.00																		
Mg	0.82	0.57	0.38	0.83	0.91	1.00																	
Be	−0.40	−0.62	0.22	−0.04	−0.53	−0.74	1.00																
Ti	−0.58	−0.39	−0.10	0.33	−0.51	−0.64	0.63	1.00															
V	0.46	0.93	−0.44	0.05	0.48	0.90	−0.80	−0.54	1.00														
Co	0.53	0.54	−0.09	0.11	0.64	0.63	−0.92	−0.63	0.77	1.00													
Ni	0.89	0.22	0.47	0.49	0.98	0.83	−0.63	−0.51	0.55	0.74	1.00												
Cu	0.92	0.15	0.56	0.36	0.93	0.97	−0.39	−0.65	0.43	0.48	0.88	1.00											
Zn	0.93	−0.07	0.75	0.24	0.81	0.69	−0.24	−0.44	0.20	0.35	0.82	0.85	1.00										
As	0.36	0.86	−0.27	0.21	0.25	0.36	−0.34	0.24	0.72	0.07	0.31	0.27	0.48	1.00									
Rb	0.04	−0.06	0.11	0.93	0.37	0.73	−0.07	0.50	0.06	0.05	0.32	0.12	0.07	0.46	1.00								
Sr	−0.60	−0.44	−0.09	−0.42	−0.85	−0.86	0.79	0.59	−0.69	−0.85	−0.85	−0.72	−0.48	−0.26	−0.33	1.00							
Y	−0.71	−0.24	−0.33	−0.57	−0.92	−0.93	0.69	0.56	−0.56	−0.70	−0.89	−0.83	−0.59	−0.16	−0.42	0.89	1.00						
Mo	0.82	0.35	0.54	0.83	0.92	0.97	−0.73	−0.75	0.77	0.68	0.83	0.98	0.66	0.12	0.65	−0.83	−0.96	1.00					
Cd	0.94	0.27	0.46	0.35	0.96	0.91	−0.61	−0.67	0.59	0.71	0.97	0.95	0.84	0.28	0.15	−0.82	−0.88	0.92	1.00				
Cs	0.45	0.50	−0.05	0.64	0.70	0.77	−0.54	−0.11	0.64	0.55	0.70	0.53	0.38	0.65	0.67	−0.81	−0.69	0.63	0.60	1.00			
Ba	0.60	0.57	−0.05	0.07	0.65	0.88	−0.74	−0.85	0.76	0.74	0.64	0.69	0.33	−0.06	−0.10	−0.74	−0.78	0.95	0.75	0.38	1.00		
W	0.66	0.08	0.59	0.99	0.92	0.76	−0.92	−0.25	0.59	0.97	0.92	0.75	0.62	0.08	0.90	−0.96	−0.92	0.79	0.84	0.76	0.61	1.00	
Tl	0.16	−0.57	0.57	−0.21	−0.02	−0.73	0.31	0.14	−0.51	−0.13	0.06	−0.03	0.41	−0.12	−0.26	0.23	0.31	−0.71	−0.02	−0.27	−0.52	−0.22	1.00
Pb	−0.63	−0.38	−0.17	−0.67	−0.88	−0.98	0.57	0.40	−0.62	−0.58	−0.82	−0.80	−0.49	−0.35	−0.56	0.88	0.93	−0.94	−0.80	−0.85	−0.70	−0.85	0.44
Bi	−0.88	−0.59	−0.43	−0.82	−0.92	−0.99	0.78	0.61	−0.93	−0.64	−0.87	−0.98	−0.78	−0.43	−0.73	0.83	0.93	−0.95	−0.94	−0.77	−0.85	−0.74	0.67
Th	−0.56	0.30	−0.67	−0.53	−0.78	−0.56	0.23	0.27	0.00	−0.44	−0.74	−0.67	−0.64	0.12	−0.32	0.67	0.64	−0.62	−0.66	−0.48	−0.25	−0.95	−0.37
U	−0.60	−0.48	−0.04	−0.32	−0.81	−0.93	0.80	0.73	−0.72	−0.83	−0.79	−0.75	−0.42	−0.13	−0.18	0.96	0.91	−0.94	−0.82	−0.68	−0.88	−0.90	0.38
La	−0.62	0.07	−0.55	−0.84	−0.85	−0.82	0.31	0.03	−0.21	−0.36	−0.82	−0.69	−0.67	−0.41	−0.76	0.67	0.79	−0.78	−0.70	−0.77	−0.25	−0.93	−0.02
Ce	−0.41	0.32	−0.61	−0.82	−0.55	−0.85	−0.21	−0.34	0.15	0.17	−0.46	−0.47	−0.54	−0.61	−0.76	0.22	0.41	−0.76	−0.36	−0.53	0.16	−0.81	−0.11
Pr	−0.65	−0.01	−0.49	−0.83	−0.87	−0.83	0.39	0.07	−0.30	−0.43	−0.85	−0.70	−0.66	−0.41	−0.75	0.71	0.83	−0.79	−0.74	−0.79	−0.33	−0.92	0.04
Nd	−0.67	−0.04	−0.48	−0.79	−0.89	−0.81	0.46	0.14	−0.35	−0.51	−0.88	−0.72	−0.68	−0.39	−0.71	0.76	0.86	−0.78	−0.77	−0.80	−0.37	−0.93	0.03
Sm	−0.70	−0.06	−0.49	−0.77	−0.92	−0.82	0.49	0.20	−0.37	−0.55	−0.91	−0.75	−0.70	−0.37	−0.67	0.79	0.88	−0.79	−0.81	−0.80	−0.42	−0.94	0.02
Eu	−0.72	−0.09	−0.47	−0.73	−0.94	−0.82	0.55	0.26	−0.41	−0.61	−0.93	−0.77	−0.71	−0.34	−0.62	0.83	0.90	−0.80	−0.84	−0.80	−0.47	−0.94	0.03
Gd	−0.71	−0.06	−0.49	−0.76	−0.93	−0.84	0.50	0.24	−0.38	−0.57	−0.92	−0.78	−0.70	−0.32	−0.65	0.81	0.90	−0.82	−0.83	−0.79	−0.46	−0.95	0.05
Tb	−0.72	−0.14	−0.43	−0.70	−0.94	−0.83	0.61	0.32	−0.47	−0.66	−0.94	−0.78	−0.69	−0.32	−0.59	0.86	0.93	−0.82	−0.86	−0.80	−0.54	−0.95	0.08
Dy	−0.72	−0.19	−0.39	−0.70	−0.95	−0.88	0.63	0.36	−0.51	−0.66	−0.93	−0.80	−0.66	−0.31	−0.58	0.88	0.96	−0.87	−0.87	−0.81	−0.60	−0.95	0.16
Ho	−0.71	−0.22	−0.35	−0.68	−0.94	−0.90	0.65	0.41	−0.53	−0.68	−0.92	−0.81	−0.63	−0.27	−0.56	0.90	0.98	−0.90	−0.87	−0.79	−0.65	−0.95	0.23
Er	−0.72	−0.29	−0.31	−0.58	−0.94	−0.91	0.73	0.51	−0.60	−0.74	−0.93	−0.82	−0.62	−0.27	−0.46	0.93	0.99	−0.91	−0.90	−0.77	−0.73	−0.94	0.24
Tm	−0.71	−0.35	−0.25	−0.47	−0.91	−0.88	0.81	0.57	−0.65	−0.82	−0.93	−0.78	−0.61	−0.30	−0.38	0.95	0.96	−0.87	−0.89	−0.76	−0.74	−0.95	0.20

Table A1. *Cont.*

	Mn	Fe	Mn/Fe	Al	Li	Mg	Be	Ti	V	Co	Ni	Cu	Zn	As	Rb	Sr	Y	Mo	Cd	Cs	Ba	W	Tl	
Yb	−0.72	−0.37	−0.23	−0.52	−0.92	−0.91	0.79	0.56	−0.67	−0.80	−0.92	−0.80	−0.60	−0.30	−0.41	0.94	0.98	−0.90	−0.90	−0.77	−0.76	−0.93	0.27	
Lu	−0.70	−0.28	−0.29	−0.58	−0.92	−0.89	0.75	0.49	−0.59	−0.75	−0.92	−0.78	−0.61	−0.29	−0.48	0.92	0.98	−0.89	−0.88	−0.77	−0.70	−0.94	0.24	
Ce an	0.27	0.55	−0.29	−0.15	0.36	0.36	−0.92	−0.65	0.70	0.93	0.47	0.23	0.07	−0.37	−0.17	−0.66	−0.51	0.51	0.47	0.27	0.72	0.83	−0.23	
Ru	0.01	−0.50	0.32	−0.80	−0.32	−0.85	0.17	−0.25	−0.48	−0.04	−0.22	−0.23	0.11	−0.45	−0.81	0.44	0.47	−0.75	−0.15	−0.72	−0.24	−0.65	0.79	
Pd	−0.50	0.17	−0.63	0.05	−0.23	−0.17	0.16	0.30	−0.09	−0.05	−0.24	−0.32	−0.44	0.11	0.18	−0.15	0.24	−0.27	−0.35	0.31	−0.36	0.02	0.03	
Ir	−0.03	0.20	−0.23	0.02	0.18	−0.16	−0.61	−0.17	0.32	0.74	0.30	−0.08	−0.09	−0.29	0.05	−0.51	−0.22	−0.10	0.17	0.28	0.21	0.50	0.16	
Pt	0.58	0.47	0.01	0.18	0.71	0.62	−0.91	−0.61	0.72	0.99	0.80	0.54	0.43	0.11	0.10	−0.88	−0.74	0.66	0.76	0.59	0.72	0.96	−0.06	
Pt/Pd	0.83	−0.17	0.99	0.30	0.78	0.48	−0.79	−0.56	0.39	0.79	0.81	0.71	0.81	−0.16	0.06	−0.55	−0.73	0.61	0.82	0.20	0.65	0.65	0.26	
	Pb	**Bi**	**Th**	**U**	**La**	**Ce**	**Pr**	**Nd**	**Sm**	**Eu**	**Gd**	**Tb**	**Dy**	**Ho**	**Er**	**Tm**	**Yb**	**Lu**	**Ce An**	**Ru**	**Pd**	**Ir**	**Pt**	**Pt/Pd**
Pb	1.00																							
Bi	0.96	1.00																						
Th	0.57	0.52	1.00																					
U	0.87	0.89	0.56	1.00																				
La	0.81	0.84	0.75	0.55	1.00																			
Ce	0.52	0.89	0.51	0.09	0.85	1.00																		
Pr	0.84	0.86	0.70	0.59	0.99	0.80	1.00																	
Nd	0.85	0.84	0.73	0.65	0.98	0.75	1.00	1.00																
Sm	0.86	0.84	0.75	0.68	0.98	0.72	0.99	1.00	1.00															
Eu	0.87	0.84	0.76	0.73	0.96	0.66	0.97	0.99	1.00	1.00														
Gd	0.88	0.86	0.77	0.72	0.97	0.70	0.98	0.99	1.00	1.00	1.00													
Tb	0.89	0.85	0.75	0.78	0.93	0.61	0.96	0.98	0.99	1.00	0.99	1.00												
Dy	0.92	0.89	0.72	0.82	0.92	0.58	0.94	0.96	0.98	0.99	0.98	1.00	1.00											
Ho	0.94	0.91	0.70	0.85	0.89	0.54	0.92	0.94	0.95	0.97	0.97	0.98	1.00	1.00										
Er	0.93	0.92	0.67	0.90	0.83	0.44	0.87	0.90	0.92	0.94	0.94	0.97	0.98	0.99	1.00									
Tm	0.89	0.89	0.64	0.92	0.76	0.33	0.81	0.86	0.88	0.91	0.90	0.94	0.95	0.96	0.99	1.00								
Yb	0.92	0.92	0.62	0.92	0.78	0.36	0.83	0.86	0.89	0.92	0.90	0.94	0.96	0.97	0.99	1.00	1.00							
Lu	0.91	0.91	0.65	0.88	0.83	0.43	0.87	0.90	0.92	0.94	0.93	0.97	0.98	0.99	1.00	0.99	0.99	1.00						
Ce an	−0.34	−0.36	−0.17	−0.70	−0.04	0.49	−0.12	−0.20	−0.25	−0.31	−0.27	−0.38	−0.40	−0.43	−0.52	−0.62	−0.60	−0.54	1.00					
Ru	0.71	-	0.15	0.43	0.58	0.74	0.56	0.52	0.49	0.45	0.49	0.45	0.50	0.52	0.47	0.38	0.44	0.46	0.23	1.00				
Pd	0.02	0.25	−0.17	−0.02	0.06	0.09	0.13	0.11	0.12	0.13	0.12	0.13	0.14	0.15	0.17	0.15	0.17	0.18	−0.14	−0.32	1.00			
Ir	−0.11	0.19	−0.38	−0.40	−0.09	0.34	−0.11	−0.18	−0.21	−0.26	−0.22	−0.29	−0.26	−0.26	−0.29	−0.39	−0.34	−0.31	0.75	0.15	0.44	1.00		
Pt	−0.62	−0.64	−0.53	−0.84	−0.46	0.07	−0.52	−0.59	−0.63	−0.68	−0.65	−0.73	−0.73	−0.74	−0.79	−0.86	−0.84	−0.80	0.88	−0.05	−0.05	0.73	1.00	
Pt/Pd	−0.46	−0.53	−0.63	−0.58	−0.59	−0.35	−0.62	−0.64	−0.67	−0.70	−0.69	−0.71	−0.69	−0.69	−0.72	−0.74	−0.72	−0.72	0.82	0.20	−0.65	0.27	0.78	1.00

Bolded values reflect significant correlation of PGE with other elements for n = 8 samples at the 95% confidence level and for n = 6 at the 90% confidence level. For Pt and Ir, n = 8; for Ru and Pd, n = 6. The Ce anomaly is calculated as Ce an = $2Ce/Ce^{PAAS}/(La/La^{PAAS} + Pr/Pr^{PAAS})$, where Ln^{PAAS} is the content in PAAS [42].

References

1. Halbach, P.E.; Jahn, A.; Cherkashov, G. Marine Co-Rich Ferromanganese Crust Deposits: Description and Formation, Occurrences and Distribution, Estimated World-wide Resources. In *Deep-Sea Mining*; Springer: Cham, Switzerland, 2017; pp. 65–141.
2. Kuhn, T.; Wegorzewski, A.; Rühlemann, C.; Vink, A. Composition, formation, and occurrence of polymetallic nodules. In *Deep-Sea Mining*; Springer: Cham, Switzerland, 2017; pp. 23–63.
3. Hein, J.R.; Mizell, K.; Koschinsky, A.; Conrad, T.A. Deep-ocean mineral deposits as a source of critical metals for high- and green-technology applications: Comparison with land-based resources. *Ore Geol. Rev.* **2013**, *51*, 1–14. [CrossRef]
4. Balaram, V.; Mathur, R.; Banakar, V.K.; Hein, J.R.; Rao, C.R.M.; Gnaneswara Rao, T.; Dasaram, B. Determination of the platinum—Group elements (PGE) and gold (Au) in manganese nodule reference samples by nickel sulfide fire-assay and Te coprecipitation with ICP-MS. *Indian J. Mar. Sci.* **2006**, *35*, 7–16.
5. Usui, A.; Someya, M. Distribution and composition of marine hydrogenetic and hydrothermal manganese deposits in the northwest Pacific. *Geol. Soc. Lond. Spec. Publ.* **1997**, *119*, 177–198. [CrossRef]
6. Halbach, P.; Kriete, C.; Prause, B.; Puteanus, D. Mechanisms to explain the platinum concentration in ferromanganese seamount crusts. *Chem. Geol.* **1989**, *76*, 95–106. [CrossRef]
7. Hein, J.R.; Mcintyre, B.; Koschinsky, A. The Global Enrichment of Platinum Group Elements in Marine Ferromanganese Crusts. *Ext. Abstr.* **2005**, *10*, 98–101.
8. Koide, M.; Stallard, M.; Hodge, V.; Goldberg, E.D. Preliminary studies on the marine chemistry of ruthenium. *Neth. J. Sea Res.* **1986**, *20*, 163–166. [CrossRef]
9. Anbar, A.D.; Wasserburg, G.J.; Papanastassiou, D.A.; Andersson, P.S. Iridium in natural waters. *Science* **1996**, *273*, 1524–1528. [CrossRef]
10. Banakar, V.K.; Hein, J.R.; Rajani, R.P.; Chodankar, A.R. Platinum group elements and gold in ferromanganese crusts from Afanasiy-Nikitin seamount, equatorial Indian Ocean: Sources and fractionation. *J. Earth Syst. Sci.* **2007**, *116*, 3–13. [CrossRef]
11. Baturin, G.N. *Geochemistry of Oceanic Ferromanganese Nodules*; Nauka: Moscow, Russia, 1986.
12. Dubinin, A.V.; Uspenskaya, T.Y. Geochemistry and specific features of manganese ore formation in sediments of oceanic bioproductive zones. *Lithol. Miner. Resour.* **2006**, *41*, 1–14. [CrossRef]
13. Dubinin, A.V. *Rare Earth Element Geochemistry in the Ocean*; Nauka: Moscow, Russia, 2006.
14. Stueben, D.; Glasby, G.P.; Eckhardt, J.-D.; Berner, Z.; Mountain, B.W.; Usui, A. Enrichments of platinum-group elements in hydrogenous, diagenetic and hydrothermal marine manganese and iron deposits. *Explor. Min. Geol.* **1999**, *8*, 233–250.
15. Cabral, A.R.; Sattler, C.D.; Lehmann, B.; Tsikos, H. Geochemistry of some marine Fe–Mn nodules and crusts with respect to Pt contents. *Resour. Geol.* **2009**, *59*, 400–406. [CrossRef]
16. Hein, J.R.; Conrad, T.; Mizell, K.; Banakar, V.K.; Frey, F.A.; Sager, W.W. Controls on ferromanganese crust composition and reconnaissance resource potential, Ninetyeast Ridge, Indian Ocean. *Deep-Sea Res. Part Oceanogr. Res. Pap.* **2016**, *110*, 1–19. [CrossRef]
17. Guan, Y.; Sun, X.; Ren, Y.; Jiang, X. Mineralogy, geochemistry and genesis of the polymetallic crusts and nodules from the South China Sea. *Ore Geol. Rev.* **2017**, *89*, 206–227. [CrossRef]
18. Muiños, S.B.; Hein, J.R.; Frank, M.; Monteiro, J.H.; Gaspar, L.; Conrad, T.; Pereira, H.G.; Abrantes, F. Deep-sea Fe–Mn Crusts from the Northeast Atlantic Ocean: Composition and Resource Considerations. *Mar. Georesour. Geotechnol.* **2013**, *31*, 40–70. [CrossRef]
19. Marino, E.; González, F.J.; Somoza, L.; Lunar, R.; Ortega, L.; Vázquez, J.T.; Reyes, J.; Bellido, E. Strategic and rare elements in Cretaceous-Cenozoic cobalt-rich ferromanganese crusts from seamounts in the Canary Island Seamount Province (northeastern tropical Atlantic). *Ore Geol. Rev.* **2017**, *87*, 41–61. [CrossRef]
20. Wen, X.; De Carlo, E.H.; Li, Y.H. Interelement relationships in ferromanganese crusts from the central Pacific ocean: Their implications for crust genesis. *Mar. Geol.* **1997**, *136*, 277–297. [CrossRef]
21. Asavin, A.M.; Kubrakova, I.V.; Mel'nikov, M.E.; Tyutyunnik, O.A.; Chesalova, E.I. Geochemical zoning in ferromanganese crusts of Ita-MaiTai guyot. *Geochem. Int.* **2010**, *48*, 423–445. [CrossRef]
22. Goldberg, E.D.; Koide, M. Understanding the marine chemistries of the platinum group metals. *Mar. Chem.* **1990**, *30*, 249–257. [CrossRef]

23. Koschinsky, A.; Audroing, J. The Enrichment of Platinum and the Fractionation of Pt from Pd in Marine Ferromanganese Crusts. *Ext. Abstr.* **2005**, *10*, 429–432.
24. Baturin, G.N.; Konopleva, E.V.; Dubinchuk, V.T.; Mel'nikov, M.E. Marine Geology-Platinum and Gold in the Ferromanganese Crusts of the Pacific Ocean. *Oceanol. Russ. Acad. Sci.* **2005**, *45*, 269–276.
25. Astakhova, N.V. Noble metals in ferromanganese crusts from marginal seas of the Northwest Pacific. *Oceanology* **2017**, *57*, 558–567. [CrossRef]
26. Glasby, G.P. Incorporation of transition and Platinum Group Elements (PGE) in Co-rich Mn crusts at Afanasiy-Nikitin Seamount (AFS) in the Equatorial S Indian Ocean. *Resour. Geol.* **2010**, *60*, 212–215. [CrossRef]
27. Kubrakova, I.V.; Koshcheeva, I.Y.; Tyutyunnik, O.A.; Asavin, A.M. Role of organic matter in the accumulation of platinum in oceanic ferromanganese deposits. *Geochem. Int.* **2010**, *48*, 655–663. [CrossRef]
28. Litvin, V.M. *The Morphostructure of the Atlantic Ocean Floor: Its Development in the Meso-Cenozoic*; Springer: Dordrecht, The Netherlands, 1984; ISBN 978-94-009-6245-3.
29. Stramma, L.; England, M. On the water masses and mean circulation of the South Atlantic Ocean. *J. Geophys. Res. Oceans* **1999**, *104*, 20863–20883. [CrossRef]
30. Shannon, L.V.; Chapman, P. Evidence of Antarctic bottom water in the Angola Basin at 32°S. *Deep Sea Res. Part A Oceanogr. Res. Pap.* **1991**, *38*, 1299–1304. [CrossRef]
31. Sval'nov, V.N.; Dmitrenko, O.B.; Kazarina, G.K.; Berezhnaya, E.D. Sedimentation in the Angola and Cape basins during the quaternary. *Lithol. Miner. Resour.* **2014**, *49*, 281–291. [CrossRef]
32. Dubinin, A.V.; Rimskaya-Korsakova, M.N. Geochemistry of rare earth elements in bottom sediments of the Brazil Basin, Atlantic Ocean. *Lithol. Miner. Resour.* **2011**, *46*, 1–16. [CrossRef]
33. Berezhnaya, E.D.; Dubinin, A.V. Determination of Platinum-Group Elements and Gold in Ferromanganese Nodule Reference Samples. *Geostand. Geoanal. Res.* **2017**, *41*, 137–145. [CrossRef]
34. Dubinin, A.V.; Sval'nov, V.N.; Berezhnaya, E.D.; Rimskaya-Korsakova, M.N.; Demidova, T.P. Geochemistry of trace and minor elements in sediments and manganese micronodules from the Angola Basin. *Lithol. Miner. Resour.* **2013**, *48*, 175–197. [CrossRef]
35. McArthur, J.M.; Howarth, R.J.; Shields, G.A. Strontium isotope stratigraphy. In *The Geologic Time Scale*; Elsevier: Cambridge, UK; 2012; pp. 127–144.
36. Dubinin, A.V.; Uspenskaya, T.Y.; Rimskaya-Korsakova, M.N.; Demidova, T.P. Rare elements and Nd and Sr isotopic composition in micronodules from the Brazil Basin, Atlantic Ocean. *Lithol. Miner. Resour.* **2017**, *52*, 81–101. [CrossRef]
37. Dubinin, A.V.; Kuznetsov, A.B.; Rimskaya-Korsakova, M.N.; Safin, T.T. Nd and Sr isotope composition in enamel of teeth from Fe–Mn nodules of the Cape Basin (Atlantic Ocean): Age and sources of matter. *Geochem. Int.* **2018**, accepted.
38. Manheim, F.T.; Lane-Bostwick, C.M. Cobalt in ferromanganese crusts as a monitor of hydrothermal discharge on the Pacific sea floor. *Nature* **1988**, *335*, 59–62. [CrossRef]
39. Frank, M.; O'Nions, R.K.; Hein, J.R.; Banakar, V.K. 60 Myr records of major elements and Pb–Nd isotopes from hydrogenous ferromanganese crusts: Reconstruction of seawater paleochemistry. *Geochim. Cosmochim. Acta* **1999**, *63*, 1689–1708. [CrossRef]
40. Bonatti, E. Classification and Genesis of Submarine Iron-Manganese Deposits. Available online: https://eurekamag.com/research/018/560/018560418.php (accessed on 28 June 2018).
41. Bau, M.; Schmidt, K.; Koschinsky, A.; Hein, J.; Kuhn, T.; Usui, A. Discriminating between different genetic types of marine ferro-manganese crusts and nodules based on rare earth elements and yttrium. *Chem. Geol.* **2014**, *381*, 1–9. [CrossRef]
42. McLennan, S.M. Rare earth elements in sedimentary rocks; influence of provenance and sedimentary processes. *Rev. Mineral. Geochem.* **1989**, *21*, 169–200.
43. Ravizza, G.E. Platinum Group Elements and their Isotopes in the Ocean. In *Encyclopedia of Ocean Sciences*, 2nd ed.; Elsevier: Cambridge, UK; 2008; pp. 494–503.
44. Terashima, S.; Mita, N.; Nakao, S.; Platinum, S.I. Platinum and palladium abundances in marine sediments and their geochemical behavior in marine environments. *Bull. Geol. Surv. Jpn.* **2002**, *53*, 725–747. [CrossRef]
45. Wedepohl, K.H. The composition of the continental crust. *Geochim. Cosmochim. Acta* **1995**, *59*, 1217–1232. [CrossRef]

46. Bézos, A.; Lorand, J.P.; Humler, E.; Gros, M. Platinum-group element systematics in Mid-Oceanic Ridge basaltic glasses from the Pacific, Atlantic, and Indian Oceans. *Geochim. Cosmochim. Acta* **2005**, *69*, 2613–2627. [CrossRef]
47. McDonough, W.F.; Sun, S.-S. The composition of the Earth. *Chem. Geol.* **1995**, *120*, 223–253. [CrossRef]
48. Falkner, K.K.; Edmond, J.M. Determination of gold at femtomolar levels in natural waters by flow-injection inductively coupled plasma quadrupole mass spectrometry. *Anal. Chem.* **1990**, *62*, 1477–1481. [CrossRef]
49. Peach, C.L.; Mathez, E.A.; Keays, R.R. Sulfide melt—Silicate melt distribution coefficients for the noble metals as deduced from MORB: Implications for partial melting. *Geochim. Cosmochim. Acta* **1990**, *54*, 3379–3389. [CrossRef]
50. Halbach, P.; Segl, M.; Puteanus, D.; Mangini, A. Co-fluxes and growth rates in ferromanganese deposits from central Pacific seamount seas. *Nature* **1983**, *304*, 716–719. [CrossRef]
51. Hein, J.R.; Schwab, W.C.; Davis, A. Cobalt- and platinum-rich ferromanganese crusts and associated substrate rocks from the Marshall Islands. *Mar. Geol.* **1988**, *78*, 255–283. [CrossRef]
52. Dubinin, A.V.; Rimskaya-Korsakova, M.N.; Berezhnaya, E.D.; Uspenskaya, T.Y.; Dara, O.M. Ferromanganese crusts of the Southern Atlantic: Evolution of composition and features of ore formation. *Geochem. Int.* **2018**, in press.
53. Cosden, J.M.; Byrne, R.H. Comparative geochemistries of PdII and PtII:. *Geochim. Cosmochim. Acta* **2003**, *67*, 1331–1338. [CrossRef]
54. Koschinsky, A.; Hein, J.R. Uptake of elements from seawater by ferromanganese crusts: Solid-phase associations and seawater speciation. *Mar. Geol.* **2003**, *198*, 331–351. [CrossRef]
55. Maeno, M.Y.; Ohashi, H.; Yonezu, K.; Miyazaki, A.; Okaue, Y.; Watanabe, K.; Ishida, T.; Tokunaga, M.; Yokoyama, T. Sorption behavior of the Pt(II) complex anion on manganese dioxide (δ-MnO_2): A model reaction to elucidate the mechanism by which Pt is concentrated into a marine ferromanganese crust. *Miner. Depos.* **2016**, *51*, 211–218. [CrossRef]
56. Moffett, J.W. A radiotracer study of cerium and manganese uptake onto suspended particles in Chesapeake Bay. *Geochim. Cosmochim. Acta* **1994**, *58*, 695–703. [CrossRef]
57. Takahashi, Y.; Shimizu, H.; Usui, A.; Kagi, H.; Nomura, M. Direct observation of tetravalent cerium in ferromanganese nodules and crusts by X-ray-absorption near-edge structure (XANES). *Geochim. Cosmochim. Acta* **2000**, *64*, 2929–2935. [CrossRef]
58. Colodner, D.C.; Boyle, E.A.; Edmond, J.M.; Thomson, J. Post-depositional mobility of platinum, iridium and rhenium in marine sediments. *Nature* **1992**, *358*, 402–404. [CrossRef]
59. Peucker-Ehrenbrink, B.; Ravizza, G. The marine osmium isotope record. *Terra Nova* **2000**, *12*, 205–219. [CrossRef]
60. Soyol-Erdene, T.O.; Huh, Y. Dissolved platinum in major rivers of East Asia: Implications for the oceanic budget. *Geochem. Geophys. Geosyst.* **2012**, *13*, 1–13. [CrossRef]
61. Cave, R.R.; Ravizza, G.E.; German, C.R.; Thomson, J.; Nesbitt, R.W. Deposition of osmium and other platinum-group elements beneath the ultramafic-hosted Rainbow hydrothermal plume. *Earth Planet. Sci. Lett.* **2003**, *210*, 65–79. [CrossRef]
62. Lee, D.S. Palladium and nickel in north-east Pacific waters. *Nature* **1983**, *305*, 47–48. [CrossRef]
63. Kuhn, T.; Bau, M.; Blum, N.; Halbach, P. Origin of negative Ce anomalies in mixed hydrothermal–hydrogenetic Fe–Mn crusts from the Central Indian Ridge. *Earth Planet. Sci. Lett.* **1998**, *163*, 207–220. [CrossRef]